JACS
JOURNAL OF THE AMERICAN CHEMICAL SOCIETY
pubs.acs.org/JACS
Article

Constructing Antiretroviral Supramolecular Polymers as Long-Acting Injectables through Rational Design of Drug Amphiphiles with Alternating Antiretroviral-Based and Hydrophobic Residues

Han Wang, Maya K. Monroe, Feihu Wang, Mingjiao Sun, Charles Flexner, and Honggang Cui*

Cite This: *J. Am. Chem. Soc.* 2023, 145, 21293−21302
Read Online

ABSTRACT: One of the main challenges in the development of long-acting injectables for HIV treatment is the limited duration of drug release, which results in the need for frequent dosing and reduced patient adherence. In this context, we leverage the intrinsic reversible features of supramolecular polymers and their unique ability to form a three-dimensional network under physiological conditions to design a class of self-assembling drug amphiphiles (DAs) based upon lamivudine, a water-soluble antiretroviral (ARV) agent and nucleoside reverse transcriptase inhibitor. The designed ARV DAs contain three pairs of alternating hydrophobic valine (V) and hydrophilic lamivudine-modified lysine (K^{3TC}) residues with a varying number of glutamic acids (E) placed on the *C*-terminus. Upon dissolution in deionized water, all three ARV DAs were found to spontaneously associate into supramolecular filaments of several micrometers in length, with varying levels of lateral stacking. Addition of 1× PBS triggered immediate gelation of the two ARV DAs with 2 or 3 E residues, and upon dilution in an *in vitro* setting, the dissociation from the supramolecular state to the monomeric state enabled a long-acting linear release of the ARV DAs. *In vivo* studies further confirmed their injectability, rapid *in situ* hydrogel formation, enhanced local retention, and long-acting therapeutic release over a month. Importantly, our pharmacokinetic studies suggest that the injected ARV supramolecular polymeric hydrogel was able to maintain a plasma concentration of lamivudine above its IC_{50} value for more than 40 days in mice and showed minimal systemic immunogenicity. We believe that these results shed important light on the rational design of long-acting injectables using the drug-based molecular assembly strategy, and the reported ARV supramolecular hydrogels hold great promise for improving HIV treatment outcomes.

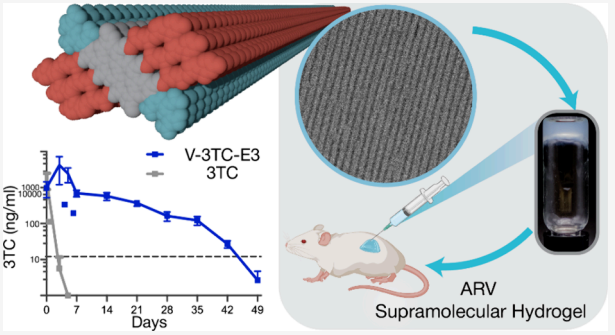

INTRODUCTION

The ability of supramolecular polymers (SPs) to percolate into a three-dimensional network in aqueous solutions enables their important use as hydrogel materials for the delivery of cells and various therapeutic compounds.[1−5] Given their biodegradable and potentially bioactive features, peptides and peptide-based conjugates, as well as peptidomimetics, have been exploited as excellent molecular building units to develop a great diversity of SPs.[5−13] Importantly, these peptide-based SPs can be designed to respond specifically to biological and biomolecular cues, solution pH, temperature, and ionic strengths, allowing their hydrogelations to occur under physiological conditions.[14−21] In most cases, molecular and macromolecular therapeutics can be physically incorporated into the hydrogel, with the release rate depending upon the diffusivity of the therapeutic compounds (largely determined by the molecular weight and size) and its affinity to the hydrogel network (e.g., associative interactions).[22,23] Recently, the design of self-assembling drug amphiphiles (DAs) allows for the creation of drug-based SPs, introducing a new means to regulate therapeutic release.[24−28] In this case, the drug release rate is primarily determined by the dissociation kinetics from the supramolecular state to the monomeric state and its consequent diffusion out of the hydrogel.[24,25] The intrinsically low dissociation rates of SP systems—that are built upon strong, associative interactions—enable sustained release of low-molecular-weight anticancer drugs over an extended period of time.[29,30] We envision that this sustained release feature could also be potentially utilized to create long-acting injectables for HIV treatment that would reduce the frequency of injections needed to maintain viral control and improve adherence to the treatment regimen.[31−33]

Over the past few decades, potent antiretroviral therapy (ART) has transformed HIV infections into a clinically manageable chronic disease.[34] Combinations of two or three

Received: May 30, 2023
Published: September 25, 2023

https://doi.org/10.1021/jacs.3c05645
J. Am. Chem. Soc. 2023, 145, 21293−21302

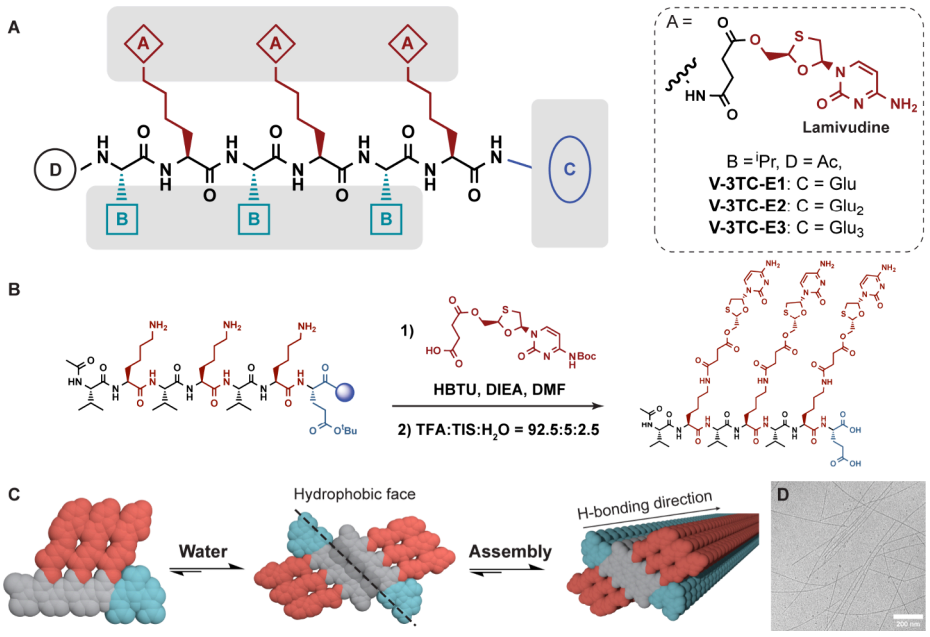

Figure 1. Molecular design and assembly of asymmetric ARV DAs. (A) Chemical structures of the three studied ARV DAs: V-3TC-E1, V-3TC-E2, and V-3TC-E3. (B) Conjugation reaction to synthesize a lamivudine prodrug containing three drug units and a hydrolyzable succinate linker. (C) Schematic illustration of the self-assembly of ARV DAs into antiparallel β-sheet tapes that further stack or entwine into filamentous nanostructures in aqueous solution. (D) Representative cryo-TEM micrograph of filaments formed by self-assembly V-3TC-E3 in water at a concentration of 1 mM, revealing filamentous nanostructures that measure 6.8 ± 1.0 nm in diameter and up to several micrometers in length.

antiretroviral (ARV) drugs, known as cART, have proven effective in suppressing plasma viral loads and preventing the progression of HIV to AIDS. However, cART is not curative and requires lifelong patient adherence. Long-acting injectable ARV regimens are highly desirable; however, most current ARV combinations rely on water-soluble nucleoside reverse transcriptase inhibitors, such as lamivudine (2′,3′-dideoxy-3′-thiacytidine, a.k.a. 3TC), whose low-molecular-weight and hydrophilic characteristics pose a great challenge to achieving long-acting delivery.[35−37] In particular, 3TC is currently used in clinic as a monotherapy to treat hepatitis B virus infections[38] and in combination with several other drugs for HIV treatment.[36,39] In this context, we report the design and synthesis of self-assembling ARV DAs by the direct linkage of the hydrophilic 3TC to the lysine side chain. Through molecular engineering of the peptide structural motif, we have developed a class of antiviral SP hydrogels for a sustained release of the hydrophilic ARV agent over 40 days *in vivo* (Figure 1).

RESULTS AND DISCUSSION

Molecular Design and Synthesis of ARV DAs. To create a series of supramolecular hydrogelators bearing hydrophilic ARV agents, we designed and synthesized three ARV DA molecules: V-3TC-E1, V-3TC-E2, and V-3TC-E3, each comprising a peptide segment with three hydrophilic 3TC moieties but differing in the number of E residues (Figure 1). We previously reported that the covalent linkage of hydrophobic drug moieties to various hydrophilic peptide segments creates a class of DAs that can spontaneously associate into therapeutic SPs in water.[25,26,29,30,40−44] To adopt this DA design strategies to achieve long-acting release of hydrophilic therapeutic agents, we incorporated the drug 3TC onto the lysine side chain through a hydrolyzable linker to create a peptide-based self-assembling motif. As shown in Figure 1A, the key design feature is the alternating VKVKVK peptide sequence, highlighting the versatility of this design platform by revealing four different types of conjugation sites for both drug anchorage and assembly modulation. Site A leverages the primary amine group of the lysine side chains for 3TC conjugation. In our design, we incorporated three 3TC conjugation sites, a decision that strikes a balance between achieving substantial drug loading—an essential factor for designing an effective long-acting ARV DA—and maintaining synthesis efficiency. 3TC moieties were conjugated via a hydrolyzable succinate linker, selected for its moderate stability to facilitate the long-acting release of the ARV DA and its straightforward synthesis protocol. Valine was chosen for site B as the hydrophobic component here due to its tendency of forming a β-sheet secondary structure (Figure 1B).[45,46] This label B is intentionally generalized to emphasize that other hydrophobic groups could be accommodated to broaden the versatility and applicability of our ARV DA design. Sites C and D provide additional conjugation points, but in this work, site C was used to modulate the assembly and gelation behavior with oligoglutamic acids, while site D was simply capped with an acetyl (Ac) group. The peptide segment of Ac-VKVKVK-E_n (n = 1−3) was synthesized using a standard Fmoc solid-phase synthesis protocol. After the *tert*-butyloxycarbonyl (Boc) protecting group was introduced, the 3TC-succinate prodrug was first synthesized and characterized by conjugating with succinate anhydride (synthesis details are discussed in the Methods section; Scheme 1 and Figures S1 and S2). The resulting prodrug was eventually grafted onto the lysine side chains (Figure 1B and Scheme S1), followed by a cleavage reaction to obtain the ARV DAs from the peptide resin. The final product was then purified using reversed-phase HPLC, and its purity and molecular mass were confirmed using analytical HPLC and ESI mass spectrometry, respectively (Figures S3−S5). The structural motif with alternating

https://doi.org/10.1021/jacs.3c05645
J. Am. Chem. Soc. 2023, 145, 21293−21302

Scheme 1. Synthesis of the Reactive 3TC Prodrug

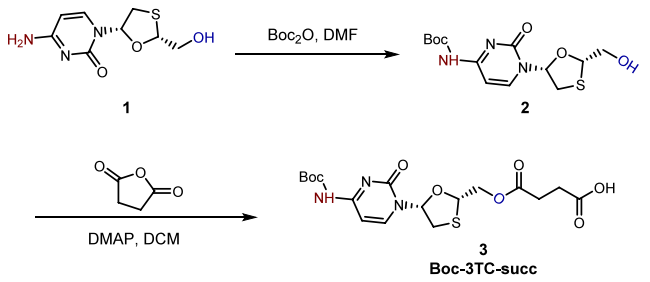

hydrophobic and hydrophilic amino acids, long known to favor β-sheet assemblies,[47] was first used by Pochan and Schneider et al. to devise a series of β-hairpin molecular hydrogelators to develop a range of biomaterials[6,10,16,48−50] and then adopted by Hartgerink et al. to construct multidomain peptides for use in tissue engineering.[51−54] In our case, it is hypothesized that the designed molecules dimerize through hydrophobic interactions between the three valine side chains before their propagation into one-dimensional (1D) assemblies via intermolecular hydrogen bonding (Figure 1C).

Nanostructure Characterization. The three ARV DAs were directly dissolved at 1 mM in deionized water (final solution pH ∼4.5) and aged for 24 h at room temperature to allow sufficient time for assembly. Transmission electron microscopy (TEM) and cryogenic TEM (cryo-TEM) imaging were then taken, revealing that all three conjugates formed 1D nanostructures over several micrometers in length (Figure 2). Twisting can be clearly seen for V-3TC-E1 and V-3TC-E2 assemblies by a closer examination of their cryo-TEM images (Figure 2A,B). The width and height of V-3TC-E1 twisted ribbons were 21.2 ± 1.2 and 6.3 ± 1.0 nm, respectively, by measuring the widest and narrowest region in Figure 2A. V-3TC-E2 assemblies in Figure 2B had a similar height of 6.1 ± 0.8 nm but a reduced width of 12.4 ± 0.8 nm. In contrast, for V-3TC-E3 filaments, the difference between their height and width can be hardly discernible, while the cryo-TEM image in Figure 2C implies some levels of twisting. Thus, we used Figure 2F to assess the diameter of V-3TC-E3 filaments, measuring 6.8 ± 1.0 nm. Clearly, the one-dimensionality of the observed assemblies is associated with the directional, intermolecular bonding among the peptide segments, as evidenced by the characteristic β-sheet absorptions around 210−216 nm in their respective circular dichroism (CD) spectra, FTIR spectra, and thioflavin T (ThT) assays (Figure S6). Given the charged nature of the E residues, all three ARV DAs are expected to assume an antiparallel β-sheet conformation in a way to lower electrostatic repulsions (Figure 1C).

The observed morphological and dimensional differences among the three ARV DA assemblies reflect the important role that the terminal glutamic acids play in modulating the lateral association of the primitive β-sheet tape, as shown in Figure 1C. Notably, our zeta potential measurements revealed that all three assemblies bear negative charges (Figure S7), suggesting that the lateral association and/or β-sheet intertwining occurred between the lysine-conjugated 3TC (K^{3TC}) faces (not the terminal glutamic acid faces), likely through combined hydrophobic interactions and $\pi-\pi$ stackings among the lysine side chain, the succinate linker, and the 3TC moiety. Given that the pK_a of the terminal cytosine of 3TC is around 7.2, 3TC is expected to be partially charged in deionized water (solution pH of around 4.5 at 1 mM), which would add some levels of electrostatic repulsions to counterbalance the associative interactions for β-sheet stacking. This cytosine-mediated stacking can be further manifested in the observed

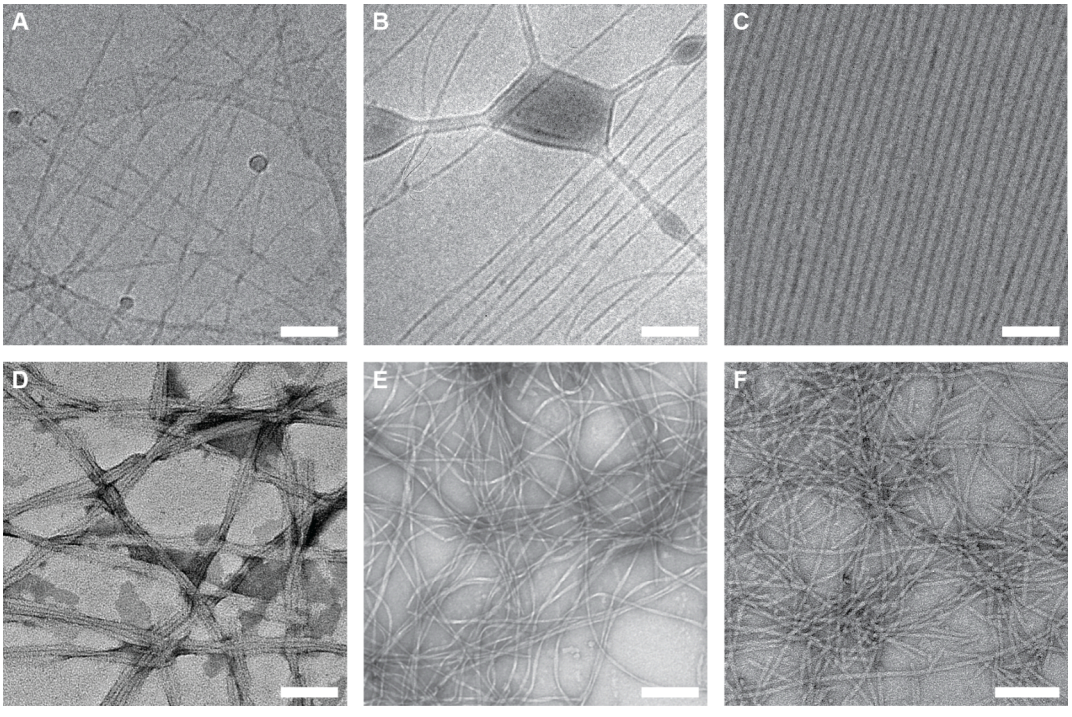

Figure 2. Self-assembly of the three studied ARV DAs in deionized water. Cryo- (A−C) and conventional (D−F) TEM micrographs of filamentous nanostructures formed by V-3TC-E1 (A, D), V-3TC-E2 (B, E), and 3TC-V-E3 (C, F) at a concentration of 1 mM. All solutions were aged for at least 24 h before measurements were taken. All scale bars are 100 nm.

https://doi.org/10.1021/jacs.3c05645
J. Am. Chem. Soc. 2023, 145, 21293−21302

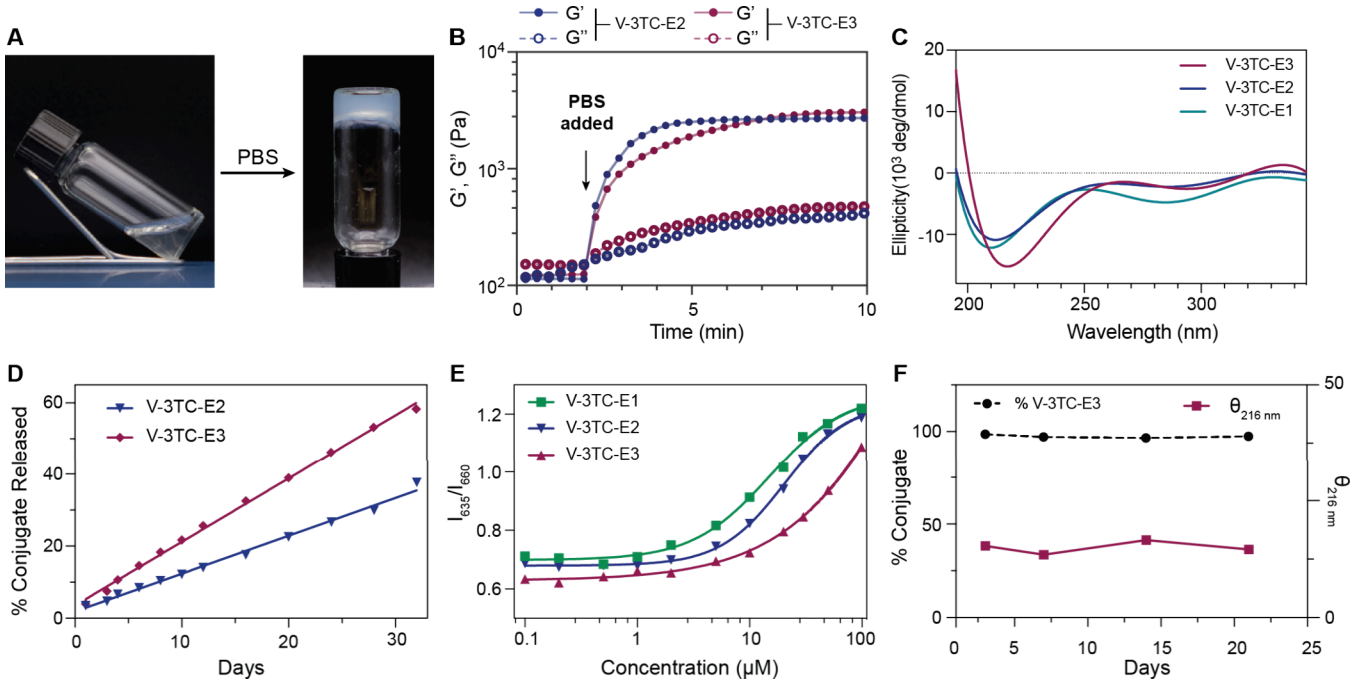

Figure 3. Gelation studies and materials characterization of lamivudine-bearing supramolecular hydrogels. (A) Photographs of solution-to-hydrogel transition of 3TC drug conjugates triggered by the addition of 1× PBS. (B) Rheological studies on the sol−gel transition process. (C) Normalized CD spectra collected between 200 and 360 nm of 3TC prodrug solutions of 200 μM after adding 1× PBS. (D) Release profile of 3TC prodrugs from ARV hydrogels taken every 2 days over a period of 1 month. Hydrogels were incubated at 37 °C. Data are given as mean ± SD (n = 3). (E) Nile red assay to measure the CMCs of the three studied 3TC prodrugs. (F) Stability tests by HPLC and CD demonstrating no noticeable *in vitro* chemical degradation observed for the 3TC conjugates over 30 days. All supramolecular hydrogels were formed at a concentration of 2 mM.

grooves for V-3TC-E1 twisted ribbons in Figure 2D, in which 2 or 3 parallel dark lines in the middle can be frequently seen, resulting from preferential deposition of uranyl acetate, the negative staining agent, during the TEM sample preparation. The distance between two neighboring dark lines is ∼6 nm, a value close to twice the length of the 3TC-modified lysine side chains. These grooves are reminiscent of those observed by the Stupp group in peptide nanobelts, where the formation of grooves and their TEM visualization were responsive to changes in solution pH.[48] Indeed, when the solution pH was raised from 4.5 to the neural pH by addition of some NaOH, these grooves disappeared (Figure S8A), indicating a change in β-sheet lateral association—due to an increased deprotonation percentage of cytosine amines—that disfavors deposition of uranyl ions. The reduced stacking from ∼21 nm in width for V-3TC-E1 assemblies to ∼12 nm for V-3TC-E2 ribbons can be attributed to the increased repulsions caused by the extra E residue. Interestingly, a further increase in the E residue constrains the lateral stacking, leading the V-3TC-E3 β-sheets to entwine into fibril-like assemblies.[55] We also found that increasing the solution pH to 7 resulted in a reduced length of all filamentous nanostructures (Figure S8), accompanied by much reduced CD signals of β-sheet absorption (Figure S6), further confirming the important role of electrostatic interactions in the studied system.[55]

Sol−Gel Transition and *In Vitro* Release. At a concentration of 2 mM or higher, solutions containing V-3TC-E2 or V-3TC-E3 assemblies can be triggered to form a hydrogel upon the addition of 1× PBS. In contrast, V-3TC-E1 did not form a hydrogel at 2 mM but instead precipitated out, likely due to its limited water solubility in the presence of salts. Using a simple vial inversion test, we determined the critical gelation concentration of V-3TC-E2 and V-3TC-E3 to be between 1.5 and 2 mM in PBS (Figure 3A). Next, we performed rheological measurements to further characterize their sol−gel transitions. Upon the addition of PBS, we found that the storage modulus (G') increased drastically to suppress the loss modulus (G'') (Figure 3B). The resultant two hydrogels showed similar mechanical properties, whereas the V-3TC-E2 solution transitioned to the gel state slightly faster. We also used CD spectrometry to probe molecular packing of the 3TC moiety within the resultant hydrogel networks. The CD spectra of the three ARV DAs after PBS addition (Figure 3C) showed a broad negative band at 274 nm that can be ascribed to lamivudine absorption (Figure S9), implying that the 3TC moieties are somehow packed in a chiral manner.

To demonstrate the long-term release behavior of the ARV-based supramolecular hydrogels, we conducted experiments to assess the *in vitro* release profiles of both V-3TC-E2 and V-3TC-E3 hydrogels at 2 mM using a previously reported method.[24,43] This experiment was intended to assess the release rate of the drug conjugate, often in the forms of monomers or short filaments, from the hydrogel depot by means of supramolecular dissociation and not to assess the release rate of the parent drug 3TC. TEM images (Figure S10) of the released supernatant revealed the presence of some short filaments (<1 μm in length). The collected medium solutions at different time points were then analyzed using HPLC to determine the amount of ARV DAs released from the hydrogel over time. As shown in Figure 3D, both hydrogels displayed a sustained linear release profile until termination of the experiments. No burst release was observed in either case. Notably, the V-3TC-E2 hydrogel exhibited a relatively lower release rate than that of V-3TC-E3. The daily release rates

https://doi.org/10.1021/jacs.3c05645
J. Am. Chem. Soc. 2023, 145, 21293−21302

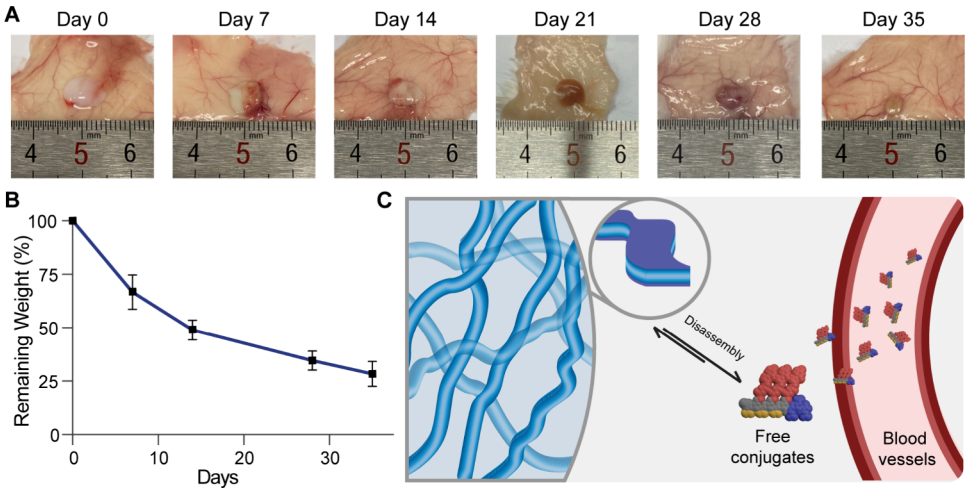

Figure 4. *In vivo* studies of hydrogel formation, local retention, and therapeutic release. (A) *In vivo* gel formation and retention assay after subcutaneous injection of a V-3TC-E3 aqueous solution in the backs of mice. (B) Long-acting release of ARV DAs reflected in the gradual reduction of hydrogels in the injection site, as determined by the remaining weight. Data are expressed as mean ± SEM (n = 5). (C) Schematic illustration of the proposed *in vivo* hydrogel release process that involves filament dissociation and the consequent diffusion of monomeric ARV DAs out of the hydrogel network.

were 1.0 and 1.9% for V-3TC-E2 and V-3TC-E3, releasing 29 and 52% of their respective conjugate over the studied period. Our previous studies suggested a strong correlation between the hydrogel *in vitro* release rate and the critical assembly concentration (CAC) value of the self-assembling constituents, with lower CAC values resulting in a slower release due to its smaller dissociation constant.[24] To validate this, we measured the CACs of the three ARV DAs using Nile red as a fluorescent probe. As shown in Figure 3E, the estimated CMC values are 5.3, 6.3, and 22.3 μM for V-3TC-E1, V-3TC-E2, and V-3TC-E3, respectively, corroborating our previous finding that CAC/CMC serves as a deterministic factor and important parameter to tune and predict the drug release rate[24] and further manifesting the role of glutamic acids in modulating their assembly in aqueous solution.

We next examined the chemical and structural stability of V-3TC-E3 when it existed in the hydrogel state (Figure 3F). The chemical stability of V-3TC-E3 was assessed using HPLC to analyze its chemical composition changes over time, and the secondary structural stability was assessed using CD. As shown in Figure 3F, the conjugate peak areas and CD signals remained nearly a constant value over 30 days, suggesting that within the hydrogel depot, no detectable chemical degradation had occurred and that the antiviral SPs did not transition into the monomeric state over time. The observed long-term stability signifies that these ARV supramolecular hydrogels can maintain their chemical identity and structural integrity over a long period of time, potentially serving as the drug depot for long-term 3TC release.

Since lamivudine is also approved by FDA for the treatment of HBV infections, we used HepAD38 cells to assess the antiviral efficacy of these ARV DAs. After the treatment of HepAD38 cells with respective ARV DAs, the cell culture supernatant was subsequently collected and analyzed by using quantitative PCR to quantify the copies of HBV DNA released from the cells (Figure S11). The IC_{50} values extrapolated from the quantitative PCR results were 0.17 μM for 3TC, 0.12 μM for V-3TC-E2, and 0.08 μM for V-3TC-E3. The results suggest potent anti-HBV activity for the ARV DAs tested, with the peptide-conjugated derivatives V-3TC-E2 and V-3TC-E3 showing enhanced antiviral potency relative to the unmodified 3TC, likely due to the improved cellular uptake associated with the conjugate design and its assembled forms.

***In Vivo* Hydrogel Breakdown and Systemic Immunogenicity.** We chose V-3TC-E3 for our *in vivo* gel retention study because it showed a higher daily release rate. Although a lower release rate may lead to prolonged release and retention in the injection site, we envision that a higher daily drug release rate might be needed to achieve and maintain a plasma drug level above the minimum effective dose of lamivudine, which could be important for drugs with a fast clearance rate. Adult BALB/cJ mice were injected subcutaneously with a solution containing 15 mM ARV DA, with PBS as a control. We observed that a hydrogel depot could be formed within 5 min after injection, while the PBS control dissipated in less than 1 h. The *in situ*-formed hydrogel gradually degraded over 5 weeks (Figure 4A). To quantitatively determine the extent of degradation over time, the amount of the remaining hydrogel was carefully scooped out and analyzed using analytic HPLC. The hydrogel exhibited roughly a linear release profile by mass, with ~22% gel remaining after 35 days (Figure 4A). The degradation rate appeared to be a bit faster at the beginning of the study, likely due to the diffusion of ARV filaments into the surroundings prior to their hydrogelation. Compared to our *in vitro* release results in Figure 3D, the hydrogel appeared to break down faster *in vivo*, which we attribute to the possible chemical degradation by enzymes and proteases in addition to the well-expected drug release pathway involving supramolecular disassembly and subsequent diffusion out of the hydrogel network (Figure 4C). While detailed analyses of the local immune response against ARV DA administration were not included in this study, the negatively charged surface of ARV DAs (Figure S7) is not expected to create potential immune clearance that contributes significantly to the drug release rate, based upon previous literature on peptide assemblies.[56,57]

To confirm the safety and tolerability of the 3TC hydrogel, we conducted experiments on complete blood counts and serum chemistry in mice after treatment. On days 28 and 56 (the study ending time), plasma and tissues were collected for

https://doi.org/10.1021/jacs.3c05645
J. Am. Chem. Soc. 2023, 145, 21293−21302

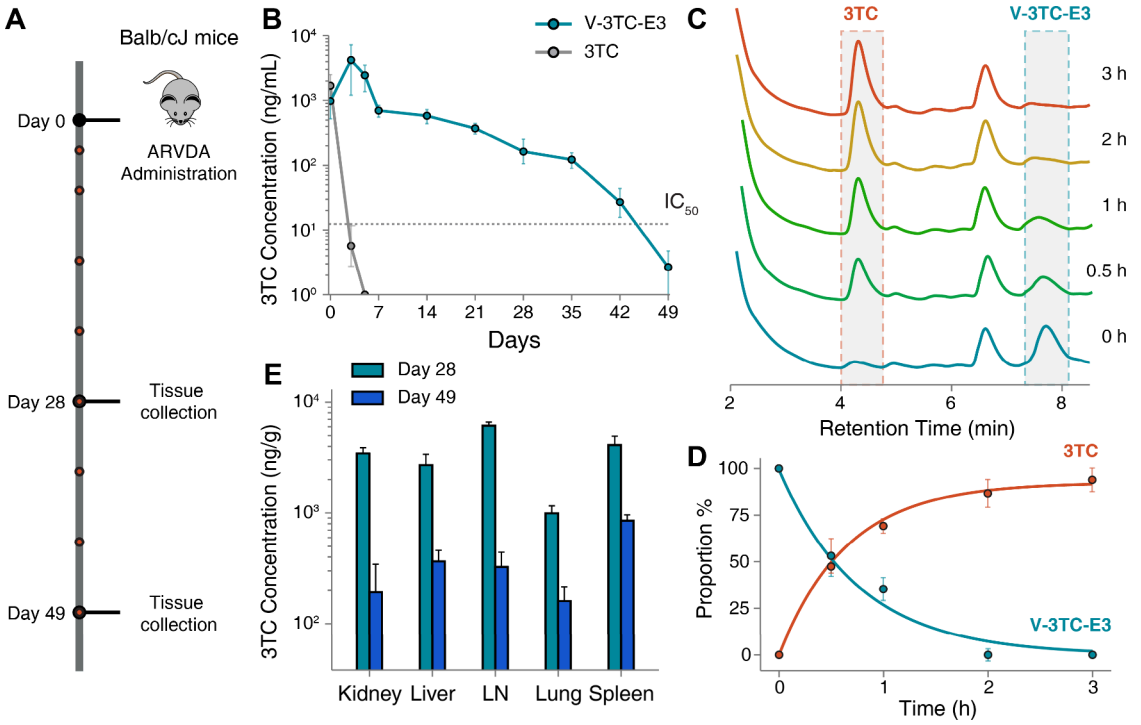

Figure 5. PK studies in BALB/cJ mice demonstrating that a high concentration of 3TC can be maintained in plasma. (A) Experimental schedule. Mice were administered 75 mg/kg equivalent of 3TC using either the parent 3TC or V-3TC-E3 conjugate. Plasma was collected for drug analysis at days 1, 3, 5, 7, 14, 21, 28, 35, 42, and 49 after treatment. (B) Plasma drug levels measured from day 0 to day 49. The dotted line indicates the IC_{50} level of 3TC. Data are expressed as mean ± SEM (n = 5). (C) HPLC chromatogram of V-3TC-E3 in mouse plasma from 0 to 3 h showing that ARV DA degrades to release free 3TC in the mouse plasma. (D) Kinetic measurement of free drug release upon degradation of V-3TC-E3 by incubation in mouse plasma for varied times before assessment with analytical RP-HPLC, showing that 3TC undergoes complete hydrolysis in plasma within 3 h. Data are presented as mean ± SEM (n = 3). (E) Drug levels in the spleen, liver, kidney, lungs, and lymph nodes (LN) on days 28 and 49 after treatment. 3TC levels were determined by UPLC-MS. Data are expressed as mean ± SEM (n = 5).

metabolic profile studies. Age-matched untreated mice were used as a control. Comprehensive serum chemistry profiles were quantified, revealing no noticeable differences between mice receiving 3TC hydrogel treatment and the untreated group (Figures S12 and S13 andTable S1). Liver and kidney metabolic profiles were unchanged, indicating that the V-3TC-E3 hydrogel was well tolerated and did not adversely affect the functions of systemic organs. Total white cell, neutrophil, lymphocyte, and monocyte counts were also unchanged during the study period. Overall, these results confirm our *in vitro* findings that the *in situ*-formed 3TC hydrogel could function as an effective self-delivery system for the sustained release of 3TC *in vivo*, without eliciting undesired systemic immune responses.

***In Vivo* Long-Acting Release.** To evaluate the pharmacokinetic (PK) and biodistribution profiles of the locally injected V-3TC-E3 hydrogel, male BALB/cJ mice were injected subcutaneously with a single dose of 75 mg/kg body weight (3TC equivalent of V-3TC-E3) (Figure 5A). Pharmaceutical standard, free 3TC, was administered at the same dosage and used as a control. Whole blood and tissue samples were collected and analyzed using ultraperformance liquid chromatography-tandem mass spectroscopy (UPLC-MS/MS) to determine parent and prodrug levels (Figure S14). In mice with free drug treatment, the 3TC plasma concentration dropped rapidly, with no drug detectable after day 3 (Figure 5B). For the group with hydrogel treatment, the 3TC concentration in plasma was observed to increase initially, reaching a maximum concentration on day 7 before it started to drop gradually. We also devised and performed *in vitro* experiments to assess the conversion of ARV DA into the parent 3TC free drug in mouse plasma (Figure S15). Figure 5C,D suggests that V-3TC-E3 started to hydrolyze into the free drug as soon as mouse plasma was introduced. After 1 h, the predominant species detected in plasma was free lamivudine, and after 3 h, the ARV DA form was nearly undetectable.

It is remarkable to note that for the ARV DA-treated group, the 3TC plasma concentrations were maintained at a level of 5-fold or higher than the IC_{50} of 3TC before day 25. Even on day 40, its plasma concentration was still above the IC_{50} level, whereas free 3TC was completely cleared after 3 days. PK parameters were determined using noncompartmental analysis for all treatment groups. The apparent 3TC half-life ($t_{1/2}$) was 27 days, 15 times longer than those of 3TC. Similarly, the mean residence time of ARV DA (38 days) was 10 times longer than that of free 3TC (2.1 days). ARV DA also resulted in tissue accumulation significantly higher than that of the free drug (Figure 5E). 3TC was undetectable in all major organs after 3 days when administered in the free 3TC form. In stark contrast, for mice treated with V-3TC-E3 hydrogels, their 3TC tissue levels on day 28 were 2337, 3453, and 4560 ng/g in the liver, spleen, and lymph node, respectively. On day 49, high tissue 3TC levels can still be detected.

CONCLUSIONS

In this work, we have designed and synthesized a series of self-assembling ARV DAs as self-formulating and self-delivering

https://doi.org/10.1021/jacs.3c05645
J. Am. Chem. Soc. 2023, 145, 21293−21302

supramolecular hydrogelators for the long-acting release of a hydrophilic ARV agent. The peptide design motif of using alternating hydrophilic and hydrophobic residues leverages the amine group of lysine side chains and the reactive *C*- and *N*-termini of short peptides to afford a versatile platform for possible conjugation of multiple types of therapeutic agents. Importantly, we demonstrated the feasibility of converting lamivudine to effective hydrogelators and their tunable assembly and gelation properties by varying the number of glutamic acid residues at the *N*-terminus. Upon the addition of PBS or subcutaneous injection, the hydrogelator-containing solutions can be triggered to gel immediately, and the resultant hydrogels exhibited long-term release of the ARV DA both *in vitro* and *in vivo*. More importantly, our results suggested that a single injection of V-3TC-E3 solution can maintain the 3TC plasma concentration above the IC_{50} level for up to 7 weeks; the ARV DA can be quickly converted to free 3TC in plasma. Our work showcases the high potential of using ARV DAs to extend the dosing intervals of ARV agents to several months or even longer after further optimization of molecular design and injected dosage. Finally, it should be noted that the reported ARV hydrogels can also be used to deliver other hydrophilic ARV agents to create a combination ART for both HIV/HBV treatment and prevention.

METHODS

Synthesis and Characterization of Boc-3TC-Succinate. 3TC (**1**, 2.00 g, 8.72 mmol) was mixed with Boc_2O (2.60 g, 12.2 mmol) in *N*,*N*-dimethylformamide (DMF). The reaction was stirred at 50 °C for 24 h. After the resulting solution was concentrated *in vacuo*, the residue was dissolved in 100 mL of dichloromethane (DCM) and washed with 100 mL of saturated $NaHCO_3$ and then with 100 mL of brine. After drying the organic layer with anhydrous $MgSO_4$ solution, the solvent was removed using a rotary evaporator, affording **2** used for the next reaction without further purification.

2 (2.68 g, 8.14 mmol), succinic anhydride (1.22 g, 12.21 mmol), and 4-dimethylaminopyridine (DMAP, 74.5 mg, 0.60 mmol) were stirred in 40 mL of anhydrous DCM. Diisopropylethylamine (DIEA, 2.10 mL, 12.2 mmol) was added to the reaction. The resulting solution was stirred at room temperature for 20 h. Water (40 mL) was charged to the solution and stirred for 1 h. The solution was then acidified with 2 M HCl to pH = 2. The crude mixture was collected by filtration and purified by flash column chromatography on silica gel to give Boc-3TC-succinate (**3**) as a white solid (1.72 g, 46% yield for the two steps). ^{1}H NMR (400 MHz, $CDCl_3$, 25 °C, ppm): 7.98 (d, J = 7.7 Hz, 1H), 7.22 (d, J = 7.6 Hz, 1H), 6.20 (t, J = 4.8 Hz, 1H), 5.43 (dd, J = 7.7, 2.5 Hz, 1H), 4.69 (dd, J = 12.2, 7.7 Hz, 1H), 4.36 (dd, J = 12.2, 2.5 Hz, 1H), 3.60 (dd, J = 12.1, 5.2 Hz, 1H), 3.08 (dd, J = 12.1, 4.3 Hz, 2H), 2.68 (s, 4H), 1.51 (s, 9H). ESI-MS calculated for $[M + H]^+$ ($C_{17}H_{24}N_3O_8S$): m/z = 430.22, found: 430.30 (Figures S1 and S2).

Synthesis and Characterization of ARV DAs. ARV DAs were synthesized on Rink Amide MBHA resin (0.5 mmol) using standard Fmoc solid-phase peptide synthesis. Fmoc deprotections were performed using 20% piperidine in DMF, and the reaction vessel was shaken for 15 min on a Burrel wrist-action shaker. This procedure was repeated one more time, and the resulting resin was washed three times with 10 mL of DMF and 10 mL of DCM. The coupling reaction was carried out by shaking the resin in a solution of HBTU (0.758 g, 2.0 mmol), Fmoc-protected amino acid (2.0 mmol), and DIEA (0.90 mL, 5.0 mmol) in 15 mL of DMF for 2 h. Acetylation was performed two times after *N*-terminal Fmoc deprotection using 15 mL of 20% Ac_2O in DMF and 100 μL of DIEA. The 4-methyltrityl (Mtt) group on the side chain of Lys(Mtt) was selectively deprotected by shaking the resin in 20 mL of TFA/TIS/DCM (3:5:92) three times. Then, **3** was conjugated onto the deprotected lysine using the same method as the amino acid coupling reaction described earlier. The peptide was cleaved with a solution of TFA/TIS/H_2O (92.5:5:2.5) for 3 h. The cleavage mixture was evaporated *in vacuo* at reduced pressure, and the crude peptide was precipitated in chilled dry diethyl ether. The crude peptide was purified using RP-HPLC with an Agilent Zorbax Extend-C18 reverse phase column (5 μm, 150 × 21.2 mm). Product identity was analyzed using ESI-MS (Figures S3−S5) and lyophilized to obtain final products as white powders. The products were redissolved, aliquoted, relyophilized, weighed, and stored at −20 °C. The purity of ARV DAs was assessed using analytical RP-HPLC with an Agilent Zorbax Extend-C18 RP column (5 μm, 150 × 4.6 mm) with a 20 μL injection volume. A linear ramping of 5−95% water/MeCN at a flow rate of 1.0 mL/min was used as the gradient condition.

Sol−Gel Transition. The ARV supramolecular hydrogels for *in vitro* studies were prepared as follows: To 180 μL of a 2.2 mM ARV DA solution in deionized water, 20 μL of 10× PBS was added 20 μL of 10× PBS to attain a final ARV DA concentration of 2 mM in PBS. Rheological experiments were conducted using an Anton Paar MCR 302 rheometer with an 8 mm parallel-plate geometry. To perform the tests, the 2.2 mM ARV DA solution (180 μL) was positioned on the sample stage, and 20 μL of 10× PBS was pipetted onto the plate's underside, situated above the material. The plate was gently lowered to the measuring position, and the storage and loss moduli (G' and G'') were recorded.

Antiviral Assay. For assessing the anti-HBV efficacy of ARV DAs, HepAD38 cells were cultured on collagen-coated 96-well flat-bottom plates at a cell density of 6×10^4 cells per well. For 3 days, cells were maintained in 200 μL of Ham's F-12K (Kaighn's) medium supplemented with 10% fetal bovine serum, 1% antibiotic solution (penicillin and streptomycin), and 0.3 mg mL^{-1} tetracycline at 37 °C in a 5% CO_2 environment. The cells were then washed and treated with a tetracycline-free medium containing H_2O, 3TC, V-3TC-E2, and V-3TC-E3. On the third day, the medium was replaced with fresh medium with the test compound at the appropriate concentration. On the fourth day, 150 μL of cell supernatant was collected and supplemented with 50 μL of nuclease-free H_2O, and DNA was extracted and eluted in 50 μL of nuclease-free water using QIAamp DNA blood mini kits (Qiagen, Germantown, MD) as per the manufacturer's instructions.

HBV DNA was quantified by qPCR, using an Integrated DNA Technologies PrimeTime Gene Expression Master Mix and HBV TaqMan primer/probe. A serial dilution of gBlocks Gene Fragments of the known HBV copy number was used as the standard for the absolute quantification of the DNA copy number from cycle threshold values. The amplification of 2 μL of aqueous DNA followed a preamplification cycle at 95 °C for 10 min, 50 cycles of 95 and 60 °C, and a melt curve in accordance with the manufacturer's protocol. The percentage of HBV production for each therapeutic concentration was determined based on the average number of copies of HBV DNA produced by water-treated cells and averaged across the three biological repeats of the assay.

***In Vitro* Drug Release and Hydrogel Stability Test.** The ARV supramolecular hydrogels were prepared, as outlined in a previous section. For measuring the *in vitro* release profiles of ARV DAs, 60 μL of PBS was placed onto the surface of a 200 μL hydrogel with a 2 mM concentration, and the sample was incubated at 37 °C. At each time point, 50 μL of PBS was carefully drawn from the gel surface and replaced with the same volume of fresh buffer.

To test the stability of ARV DA in supramolecular hydrogels, a 200 μL hydrogel sample with a 2 mM concentration was incubated at 37 °C. At each predetermined time point, a 25 μL portion of hydrogel was extracted, diluted 10-fold with PBS, and then prepared for CD and HPLC analysis.

The ARV DA concentration and purity were determined using RP-HPLC on an Agilent Zorbax Extend-C18 RP column (5 μm, 150 × 4.6 mm) with an injection volume of 20 μL. The gradient condition was a linear ramping of 5−95% water/MeCN at a flow rate of 1.0 mL/min.

V-3TC-E3 Degradation in Mice Plasma. Drug release studies of V-3TC-E3 were performed at a concentration of 200 μM in PBS

https://doi.org/10.1021/jacs.3c05645
J. Am. Chem. Soc. 2023, 145, 21293−21302

buffer with mouse plasma (10% v/v). Briefly, 400 μM stock solutions of V-3TC-E3 in PBS were prepared and aged overnight. Stock solutions of 10% v/v mouse plasma in PBS were prepared 30 min before the experiment. Three replicates of V-3TC-E3 solutions were prepared by mixing the two stock solutions in a 1:1 ratio and were incubated at 37 °C. Samples were collected at 0, 0.5, 1, 2, and 3 h, diluted with PBS by 10-fold, snap frozen with liquid nitrogen, and stored at −30 °C. The release profile was determined by analytical RP-HPLC using the following conditions: RP-HPLC on an Agilent Zorbax Extend-C18 RP column (5 μm, 150 × 4.6 mm) with an injection volume of 20 μL. The gradient condition was a linear ramping of 5−95% water/MeCN at a flow rate of 1.0 mL/min.

***In Vivo* Hydrogel Degradation.** Five male BALB/cJ mice, aged between 8 and 10 weeks, were subcutaneously injected with 140 μL of a 15 mM V-3TC-E3 solution. This dosage equates to a 3TC equivalent of 75 mg/kg. We subcutaneously injected the V-3TC-E3 solution into the backs of mice, chosen for its larger surface area and minimal mechanical disruption, allowing for a more reliable assessment of the hydrogel's long-term stability and drug release profiles. The mice were photographed and sacrificed at different time intervals (days 0, 1, 7, 14, 28, 35, and 42). The remaining hydrogel sample was photographed and carefully collected and dissolved in water/MeCN 8:2. The concentration of the remaining drug was determined by using HPLC to calculate the remaining weights of the undegraded hydrogel.

***In Vivo* PK and Biodistribution.** Five male BALB/cJ mice, aged between 8 and 10 weeks, were subcutaneously injected with 140 μL of a 15 mM V-3TC-E3 solution. This dosage equates to a 3TC equivalent of 75 mg/kg. The whole blood sample was collected at 1, 3, 5, 7, 14, 21, 28, 35, 42, and 49 days after administration. At days 28 and 56, animals were humanely euthanized, and tissues (liver, lung, lymph nodes, kidneys, and spleen) were collected for quantitative drug analysis.

For blood analysis, plasma was prepared by centrifugation of blood collected in heparinized tubes at 2000 × *g* for 5 min. 3TC and V-3TC-E3 were extracted from plasma (20 μL) using 1 mL of acetonitrile. Ten microliters of 500 ng/mL emtricitabine solution was added to each sample as an internal standard (IS), which gave a final IS concentration of 50 ng/mL after reconstitution. Samples were dried under a N_2 stream and reconstituted in 100 μL of 80% v/v LC-MS-grade MeOH/H_2O. Ten microliters of the sample solution was injected into a Waters Acquity/Xevo-G2 UPLC/MS system (Milford, MA) for analysis.

For tissue analysis, an optimized amount of tissue sample was processed using a tissue homogenizer in 5 volumes of 90% v/v LC/MS-grade MeCN/H_2O. Tissue homogenate (100 μL) was mixed with 90 μL of 90% v/v LC/MS-grade MeCN/H_2O, 10 μL of LC-MS-grade water, and 10 μL of 500 ng/mL emtricitabine solution (as an IS). After extraction, 10 μL of the sample solution was injected into a Waters Acquity/Xevo-G2 UPLC/MS system (Milford, MA) for analysis.

Standard curves of 3TC or V-3TC-E3 were prepared in blank mouse plasma in the range of 0.7−7000 and 0.25−2500 ng/mL of corresponding compounds, respectively. Emtricitabine solution was added to each sample as an IS to give a final IS concentration of 50 ng/mL. Quantitative analysis was performed based upon the ratio of 3TC peak area and IS peak area.

■ ASSOCIATED CONTENT

Supporting Information

The Supporting Information is available free of charge at https://pubs.acs.org/doi/10.1021/jacs.3c05645.

Materials, synthesis details, and experimental methods; chemical characterization and supporting figures (Scheme S1, Table S1, and Figures S1−S15) (PDF)

■ AUTHOR INFORMATION

Corresponding Author

Honggang Cui − *Department of Chemical and Biomolecular Engineering and Institute for NanoBioTechnology and Department of Materials Science and Engineering, The Johns Hopkins University, Baltimore, Maryland 21218, United States; Department of Oncology and Sidney Kimmel Comprehensive Cancer Center, Johns Hopkins University School of Medicine, Baltimore, Maryland 21205, United States;* orcid.org/0000-0002-4684-2655; Email: hcui6@jhu.edu

Authors

Han Wang − *Department of Chemical and Biomolecular Engineering and Institute for NanoBioTechnology, The Johns Hopkins University, Baltimore, Maryland 21218, United States*

Maya K. Monroe − *Department of Chemical and Biomolecular Engineering and Institute for NanoBioTechnology, The Johns Hopkins University, Baltimore, Maryland 21218, United States;* orcid.org/0000-0002-8161-5298

Feihu Wang − *Department of Chemical and Biomolecular Engineering and Institute for NanoBioTechnology, The Johns Hopkins University, Baltimore, Maryland 21218, United States;* orcid.org/0000-0002-0358-967X

Mingjiao Sun − *Department of Chemical and Biomolecular Engineering and Institute for NanoBioTechnology, The Johns Hopkins University, Baltimore, Maryland 21218, United States*

Charles Flexner − *Division of Clinical Pharmacology and Infectious Diseases, Johns Hopkins University School of Medicine and Bloomberg School of Public Health, Baltimore, Maryland 21205, United States*

Complete contact information is available at: https://pubs.acs.org/10.1021/jacs.3c05645

Notes

The authors declare no competing financial interest.

■ ACKNOWLEDGMENTS

The work is supported by the Johns Hopkins University Center for AIDS Research (JHU CFAR) under NIH/NIAID P30AI094189. We acknowledge the Johns Hopkins University (JHU) Integrated Imaging Center (IIC) for the use of the TEM facility, the JHU Department of Chemistry NMR facility, and the JHU Department of Chemistry MS facility.

■ REFERENCES

(1) Aida, T.; Meijer, E. W.; Stupp, S. I. Functional Supramolecular Polymers. *Science* **2012**, *335* (6070), 813−817.
(2) Webber, M. J.; Appel, E. A.; Meijer, E. W.; Langer, R. Supramolecular biomaterials. *Nat. Mater.* **2016**, *15* (1), 13−26.
(3) Zhao, F.; Ma, M. L.; Xu, B. Molecular hydrogels of therapeutic agents. *Chem. Soc. Rev.* **2009**, *38* (4), 883−891.
(4) Lindsey, S.; Piatt, J. H.; Worthington, P.; Sonmez, C.; Satheye, S.; Schneider, J. P.; Pochan, D. J.; Langhans, S. A. Beta Hairpin Peptide Hydrogels as an Injectable Solid Vehicle for Neurotrophic Growth Factor Delivery. *Biomacromolecules* **2015**, *16* (9), 2672−2683.
(5) Webber, M. J.; Matson, J. B.; Tamboli, V. K.; Stupp, S. I. Controlled release of dexamethasone from peptide nanofiber gels to modulate inflammatory response. *Biomaterials* **2012**, *33* (28), 6823−32.

(6) Majumder, P.; Singh, A.; Wang, Z.; Dutta, K.; Pahwa, R.; Liang, C.; Andrews, C.; Patel, N. L.; Shi, J.; Val, N. d.; Walsh, S. T. R.; Jeon, A. B.; Karim, B.; Hoang, C. D.; Schneider, J. P. Surface-fill hydrogel attenuates the oncogenic signature of complex anatomical surface cancer in a single application. *Nat. Nanotechnol.* **2021**, *16*, 1−9.
(7) Batra, R.; Loeffler, T. D.; Chan, H.; Srinivasan, S.; Cui, H.; Korendovych, I. V.; Nanda, V.; Palmer, L. C.; Solomon, L. A.; Fry, H. C.; Sankaranarayanan, S. K. R. S. Machine learning overcomes human bias in the discovery of self-assembling peptides. *Nat. Chem.* **2022**, *14*, 1427−1435, DOI: 10.1038/s41557-022-01055-3.
(8) Cui, H.; Webber, M. J.; Stupp, S. I. Self-assembly of peptide amphiphiles: From molecules to nanostructures to biomaterials. *Biopolymers* **2010**, *94* (1), 1−18.
(9) Stern, D.; Cui, H. Crafting Polymeric and Peptidic Hydrogels for Improved Wound Healing. *Adv. Healthcare Mater.* **2019**, *8* (9), 1900104.
(10) Schneider, J. P.; Pochan, D. J.; Ozbas, B.; Rajagopal, K.; Pakstis, L.; Kretsinger, J. Responsive Hydrogels from the Intramolecular Folding and Self-Assembly of a Designed Peptide. *J. Am. Chem. Soc.* **2002**, *124* (50), 15030−15037.
(11) Nowak, A. P.; Breedveld, V.; Pakstis, L.; Ozbas, B.; Pine, D. J.; Pochan, D.; Deming, T. J. Rapidly recovering hydrogel scaffolds from self-assembling diblock copolypeptide amphiphiles. *Nature* **2002**, *417* (6887), 424−428.
(12) Song, J.; Yuan, C.; Jiao, T.; Xing, R.; Yang, M.; Adams, D. J.; Yan, X. Multifunctional Antimicrobial Biometallohydrogels Based on Amino Acid Coordinated Self-Assembly. *Small* **2020**, *16* (8), 1907309.
(13) Black, K. A.; Lin, B. F.; Wonder, E. A.; Desai, S. S.; Chung, E. J.; Ulery, B. D.; Katari, R. S.; Tirrell, M. V. Biocompatibility and Characterization of a Peptide Amphiphile Hydrogel for Applications in Peripheral Nerve Regeneration. *Tissue Eng. Part A* **2015**, *21* (7−8), 1333−1342.
(14) Acar, H.; Ting, J. M.; Srivastava, S.; LaBelle, J. L.; Tirrell, M. V. Molecular engineering solutions for therapeutic peptide delivery. *Chem. Soc. Rev.* **2017**, *46* (21), 6553−6569.
(15) Tantakitti, F.; Boekhoven, J.; Wang, X.; Kazantsev, R. V.; Yu, T.; Li, J.; Zhuang, E.; Zandi, R.; Ortony, J. H.; Newcomb, C. J.; Palmer, L. C.; Shekhawat, G. S.; Cruz, M. O. d. l.; Schatz, G. C.; Stupp, S. I. Energy landscapes and functions of supramolecular systems. *Nat. Mater.* **2016**, *15* (4), 469−476.
(16) Haines-Butterick, L.; Rajagopal, K.; Branco, M.; Salick, D.; Rughani, R.; Pilarz, M.; Lamm, M. S.; Pochan, D. J.; Schneider, J. P. Controlling hydrogelation kinetics by peptide design for three-dimensional encapsulation and injectable delivery of cells. *Proc. Natl. Acad. Sci. U.S.A.* **2007**, *104* (19), 7791−7796.
(17) Hule, R. A.; Nagarkar, R. P.; Hammouda, B.; Schneider, J. P.; Pochan, D. J. Dependence of Self-Assembled Peptide Hydrogel Network Structure on Local Fibril Nanostructure. *Macromolecules* **2009**, *42* (18), 7137−7145.
(18) Du, X.; Zhou, J.; Shi, J.; Xu, B. Supramolecular hydrogelators and Hydrogels: From Soft Matter to Molecular Biomaterials. *Chem. Rev.* **2015**, *115* (24), 13165−13307.
(19) Schiapparelli, P.; Zhang, P.; Lara-Velazquez, M.; Guerrero-Cazares, H.; Lin, R.; Su, H.; Chakroun, R. W.; Tusa, M.; Quiñones-Hinojosa, A.; Cui, H. Self-assembling and self-formulating prodrug hydrogelator extends survival in a glioblastoma resection and recurrence model. *J. Controlled Release* **2020**, *319*, 311−321.
(20) Li, Z.; Zhu, Y.; Matson, J. B. pH-Responsive Self-Assembling Peptide-Based Biomaterials: Designs and Applications. *ACS Appl. Bio Mater.* **2022**, *5* (10), 4635−4651.
(21) Ding, Y.; Zheng, D.; Xie, L.; Zhang, X.; Zhang, Z.; Wang, L.; Hu, Z. W.; Yang, Z. Enzyme-Instructed Peptide Assembly Favored by Preorganization for Cancer Cell Membrane Engineering. *J. Am. Chem. Soc.* **2023**, *145* (8), 4366−4371.
(22) Wang, F.; Huang, Q.; Su, H.; Sun, M.; Wang, Z.; Chen, Z.; Zheng, M.; Chakroun, R. W.; Monroe, M. K.; Chen, D.; Wang, Z.; Gorelick, N.; Serra, R.; Wang, H.; Guan, Y.; Suk, J. S.; Tyler, B.; Brem, H.; Hanes, J.; Cui, H. Self-assembling paclitaxel-mediated stimulation of tumor-associated macrophages for postoperative treatment of glioblastoma. *Proc. Natl. Acad. Sci. U.S.A.* **2023**, *120* (18), No. e2204621120.
(23) Wang, F.; Su, H.; Wang, Z.; Anderson, C. F.; Sun, X.; Wang, H.; Laffont, P.; Hanes, J.; Cui, H. Supramolecular Filament Hydrogel as a Universal Immunomodulator Carrier for Immunotherapy Combinations. *ACS Nano* **2023**, *17* (11), 10651−10664.
(24) Chakroun, R. W.; Wang, F.; Lin, R.; Wang, Y.; Su, H.; Pompa, D.; Cui, H. Fine-Tuning the Linear Release Rate of Paclitaxel-Bearing Supramolecular Filament Hydrogels through Molecular Engineering. *ACS Nano* **2019**, *13* (7), 7780−7790.
(25) Cheetham, A. G.; Zhang, P.; Lin, Y.-A.; Lock, L. L.; Cui, H. Supramolecular nanostructures Formed by Anticancer Drug Assembly. *J. Am. Chem. Soc.* **2013**, *135* (8), 2907−2910.
(26) Wang, F.; Su, H.; Xu, D.; Dai, W.; Zhang, W.; Wang, Z.; Anderson, C. F.; Zheng, M.; Oh, R.; Wan, F.; Cui, H. Tumour sensitization via the extended intratumoural release of a STING agonist and camptothecin from a self-assembled hydrogel. *Nat. Biomed. Eng.* **2020**, *4* (11), 1090−1101.
(27) Wang, H.; Monroe, M.; Leslie, F.; Flexner, C.; Cui, H. Supramolecular nanomedicines through rational design of self-assembling prodrugs. *Trends Pharmacol. Sci.* **2022**, *43* (6), 510−521.
(28) Sis, M. J.; Ye, Z.; La Costa, K.; Webber, M. J. Energy Landscapes of Supramolecular Peptide-Drug Conjugates Directed by Linker Selection and Drug Topology. *ACS Nano* **2022**, *16* (6), 9546−9558.
(29) Wang, F.; Xu, D.; Su, H.; Zhang, W.; Sun, X.; Monroe, M. K.; Chakroun, R. W.; Wang, Z.; Dai, W.; Oh, R.; Wang, H.; Fan, Q.; Wan, F.; Cui, H. Supramolecular prodrug hydrogelator as an immune booster for checkpoint blocker−based immunotherapy. *Sci. Adv.* **2020**, *6* (18), No. eaaz8985.
(30) Wang, H.; Monroe, M.; Leslie, F.; Flexner, C.; Cui, H. Supramolecular nanomedicines through rational design of self-assembling prodrugs. *Trends Pharmacol. Sci.* **2022**, *43*, 510−521, DOI: 10.1016/j.tips.2022.03.003.
(31) Monroe, M.; Flexner, C.; Cui, H. Harnessing nanostructured systems for improved treatment and prevention of HIV disease. *Bioeng. Transl. Med.* **2018**, *3* (2), 102−123.
(32) Monroe, M. K.; Wang, H.; Anderson, C. F.; Jia, H.; Flexner, C.; Cui, H. Leveraging the therapeutic, biological, and self-assembling potential of peptides for the treatment of viral infections. *J. Controlled Release* **2022**, *348*, 1028−1049.
(33) Monroe, M. K.; Wang, H.; Anderson, C. F.; Qin, M.; Thio, C. L.; Flexner, C.; Cui, H. Antiviral supramolecular polymeric hydrogels by self-assembly of tenofovir-bearing peptide amphiphiles. *Biomater. Sci.* **2023**, *11* (2), 489−498.
(34) Palella, F. J.; Delaney, K. M.; Moorman, A. C.; Loveless, M. O.; Fuhrer, J.; Satten, G. A.; Aschman, D. J.; Holmberg, S. D. Declining morbidity and mortality among patients with advanced human immunodeficiency virus infection. *N. Engl. J. Med.* **1998**, *338* (13), 853−860.
(35) Cobb, D. A.; Smith, N. A.; Edagwa, B. J.; McMillan, J. M. Long-acting approaches for delivery of antiretroviral drugs for prevention and treatment of HIV: a review of recent research. *Expert Opin. Drug Delivery* **2020**, *17* (9), 1227−1238.
(36) Gallant, J. E.; DeJesus, E.; Arribas, J. R.; Pozniak, A. L.; Gazzard, B.; Campo, R. E.; Lu, B.; McColl, D.; Chuck, S.; Enejosa, J.; Toole, J. J.; Cheng, A. K. Tenofovir DF, emtricitabine, and efavirenz vs. zidovudine, lamivudine, and efavirenz for HIV. *N. Engl. J. Med.* **2006**, *354* (3), 251−260.
(37) Kulkarni, T. A.; Bade, A. N.; Sillman, B.; Shetty, B. L. D.; Wojtkiewicz, M. S.; Gautam, N.; Hilaire, J. R.; Sravanam, S.; Szlachetka, A.; Lamberty, B. G.; Morsey, B. M.; Fox, H. S.; Alnouti, Y.; McMillan, J. M.; Mosley, R. L.; Meza, J.; Domanico, P. L.; Yue, T.-Y.; Moore, G.; Edagwa, B. J.; Gendelman, H. E. A year-long extended release nanoformulated cabotegravir prodrug. *Nat. Mater.* **2020**, *19*, 910−920, DOI: 10.1038/s41563-020-0674-z.
(38) Liaw, Y. F.; Sung, J. J. Y.; Chow, W. C.; Farrell, G.; Lee, C. Z.; Yuen, H.; Tanwandee, T.; Tao, Q. M.; Shue, K.; Keene, O. N.; Dixon,

J. S.; Gray, D. F.; Sabbat, J. Lamivudine for patients with chronic hepatitis B and advanced liver disease. *N. Engl. J. Med.* **2004**, *351* (15), 1521−1531.
(39) Sax, P. E.; Tierney, C.; Collier, A. C.; Fischl, M. A.; Mollan, K.; Peeples, L.; Godfrey, C.; Jahed, N. C.; Myers, L.; Katzenstein, D.; Farajallah, A.; Rooney, J. F.; Ha, B.; Woodward, W. C.; Koletar, S. L.; Johnson, V. A.; Geiseler, P. J.; Daar, E. S. Abacavir-Lamivudine versus Tenofovir-Emtricitabine for Initial HIV-1 Therapy. *N. Engl. J. Med.* **2009**, *361* (23), 2230−2240.
(40) Su, H.; Zhang, W.; Wang, H.; Wang, F.; Cui, H. Paclitaxel-Promoted Supramolecular Polymerization of Peptide Conjugates. *J. Am. Chem. Soc.* **2019**, *141* (30), 11997−12004.
(41) Su, H.; Wang, F.; Ran, W.; Zhang, W.; Dai, W.; Wang, H.; Anderson, C. F.; Wang, Z.; Zheng, C.; Zhang, P.; Li, Y.; Cui, H. The role of critical micellization concentration in efficacy and toxicity of supramolecular polymers. *Proc. Natl. Acad. Sci. U.S.A.* **2020**, *117* (9), 4518−4526.
(42) Su, H.; Wang, F.; Wang, Y.; Cheetham, A. G.; Cui, H. Macrocyclization of a Class of Camptothecin Analogues into Tubular Supramolecular Polymers. *J. Am. Chem. Soc.* **2019**, *141* (43), 17107−17111.
(43) Chakroun, R. W.; Sneider, A.; Anderson, C. F.; Wang, F.; Wu, P.; Wirtz, D.; Cui, H. Supramolecular Design of Unsymmetric Reverse Bolaamphiphiles for Cell-Sensitive Hydrogel Degradation and Drug Release. *Angew. Chem., Int. Ed.* **2020**, *59* (11), 4434−4442.
(44) Su, H.; Wang, F.; Wang, H.; Zhang, W.; Anderson, C. F.; Cui, H. Propagation-Instigated Self-Limiting Polymerization of Multi-armed Amphiphiles into Finite Supramolecular Polymers. *J. Am. Chem. Soc.* **2021**, *143* (44), 18446−18453.
(45) Cui, H.; Cheetham, A. G.; Pashuck, E. T.; Stupp, S. I. Amino Acid Sequence in Constitutionally Isomeric Tetrapeptide Amphiphiles Dictates Architecture of One-Dimensional nanostructures. *J. Am. Chem. Soc.* **2014**, *136* (35), 12461−12468.
(46) Cui, H.; Muraoka, T.; Cheetham, A. G.; Stupp, S. I. Self-Assembly of Giant Peptide Nanobelts. *Nano Lett.* **2009**, *9* (3), 945−951.
(47) Brack, A.; Caille, A. Synthesis and β-Conformation of Copolypeptides With Alternating Hydrophilic and Hydrophobic Residues. *Int. J. Pept. Protein Res.* **1978**, *11* (2), 128−139.
(48) Lamm, M. S.; Rajagopal, K.; Schneider, J. P.; Pochan, D. J. Laminated morphology of nontwisting β-sheet fibrils constructed via peptide self-assembly. *J. Am. Chem. Soc.* **2005**, *127* (47), 16692−16700.
(49) Pochan, D. J.; Schneider, J. P.; Kretsinger, J.; Ozbas, B.; Rajagopal, K.; Haines, L. Thermally reversible hydrogels via intramolecular folding and consequent self-assembly of a de Novo designed peptide. *J. Am. Chem. Soc.* **2003**, *125* (39), 11802−11803.
(50) Salick, D. A.; Kretsinger, J. K.; Pochan, D. J.; Schneider, J. P. Inherent antibacterial activity of a peptide-based β-hairpin hydrogel. *J. Am. Chem. Soc.* **2007**, *129* (47), 14793−14799.
(51) Beniash, E.; Hartgerink, J. D.; Storrie, H.; Stendahl, J. C.; Stupp, S. I. Self-assembling peptide amphiphile nanofiber matrices for cell entrapment. *Acta Biomater.* **2005**, *1* (4), 387−97.
(52) Dong, H.; Paramonov, S. E.; Aulisa, L.; Bakota, E. L.; Hartgerink, J. D. Self-assembly of multidomain peptides: Balancing molecular frustration controls conformation and nanostructure. *J. Am. Chem. Soc.* **2007**, *129* (41), 12468−12472.
(53) Galler, K. M.; Aulisa, L.; Regan, K. R.; D'Souza, R. N.; Hartgerink, J. D. Self-Assembling multidomain Peptide Hydrogels: Designed Susceptibility to Enzymatic Cleavage Allows Enhanced Cell Migration and Spreading. *J. Am. Chem. Soc.* **2010**, *132* (9), 3217−3223.
(54) Pogostin, B. H.; Yu, M. H.; Azares, A. R.; Euliano, E. M.; Lai, C. S. E.; Saenz, G.; Wu, S. X.; Farsheed, A. C.; Melhorn, S. M.; Graf, T. P.; Woodside, D. G.; Hartgerink, J. D.; McHugh, K. J. multidomain peptide hydrogel adjuvants elicit strong bias towards humoral immunity. *Biomater. Sci.* **2022**, *10* (21), 6217−6229.
(55) Hu, Y.; Lin, R.; Zhang, P.; Fern, J.; Cheetham, A. G.; Patel, K.; Schulman, R.; Kan, C.; Cui, H. Electrostatic-driven lamination and untwisting of β-sheet assemblies. *ACS Nano* **2016**, *10* (1), 880−888.
(56) Wen, Y.; Waltman, A.; Han, H.; Collier, J. H. Switching the immunogenicity of Peptide Assemblies Using Surface Properties. *ACS Nano* **2016**, *10* (10), 9274−9286.
(57) Fromen, C. A.; Robbins, G. R.; Shen, T. W.; Kai, M. P.; Ting, J. P.; DeSimone, J. M. Controlled analysis of nanoparticle charge on mucosal and systemic antibody responses following pulmonary immunization. *Proc. Natl. Acad. Sci. U.S.A.* **2015**, *112* (2), 488−493.

https://doi.org/10.1021/jacs.3c05645
J. Am. Chem. Soc. 2023, 145, 21293−21302